# One-step wet-spinning process of CB/CNT/MnO2 nanotubes hybrid flexible fibres as electrodes for wearable supercapacitors

**Garcia-Torres, J., Roberts, A. J., Slade, R. C. T. & Crean, C.**



DOI 10.1016/j.electacta.2018.10.201
ISSN 0013-4686

Publisher: Elsevier

# One-step wet-spinning process of CB/CNT/$MnO_2$ nanotubes hybrid flexible fibres as electrodes for wearable supercapacitors

Jose Garcia-Torres[a,1,*], Alexander J. Roberts[a,2], Robert C.T. Slade[a], Carol Crean[a]

[a] Department of Chemistry, University of Surrey, Guildford, Surrey, GU2 7XH, United Kingdom

[1] now Serra Húnter Fellow at Department of Materials Science and Metallurgical Engineering, Universitat Politècnica de Catalunya, Barcelona, 08019, Spain

[2] now at WMG, International Manufacturing Centre, University of Warwick, Coventry, CV4 7AL, United Kingdom

*Corresponding author:
e-mails: jose.manuel.garcia-torres@upc.edu

## ABSTRACT

Fibres made from different nanostructured carbons (carbon black (CB)), carbon nanotubes (CNT) and CB/CNT were successfully developed by wet-spinning. The variation of dispersion conditions (carbon nanomaterial concentration, dispersant/Carbon nanomaterial concentration ratio, CB/CNT concentration ratio, pH) resulted in different electrochemical performance for each type of fibres. Fibres with the best capacitance values (10 F $g^{-1}$) and good cycling stability (89%) were obtained from fibres containing 10% carbon black and 90% carbon nanotubes. A solid-state supercapacitor was fabricated by assembling the CB/CNT fibres resulting in 9.2 F $g^{-1}$ electrode capacitance. Incorporation of 0.2 wt.% birnessite-type potassium manganese oxide nanotubes dramatically increased the capacitance of the fibres up to 246 F $g^{-1}$ due to the high specific capacitance of birnessite phase and the tubular nature of the nanomaterial.

*Keywords: carbon nanomaterials, birnessite $MnO_2$ nanotubes, wet-spinning, flexible fibre, solid-state supercapacitor*

## 1. Introduction

Flexible and wearable electronic devices have recently attracted a great deal of interest for their potential application in personal electronics or healthcare, including roll-up and bendable displays, portable electronic papers, sensors and actuators [1-4]. Moreover, the energy storage devices that power such devices should also be flexible and wearable for truly real applications. Among the different energy storage devices, electrochemical fibre-shaped supercapacitors are increasingly investigated due to their excellent electrochemical performance (high power density, long cycle life, fast charge-discharge rate [5-7]) as well as their flexible and lightweight nature showing promising possibilities to fully integrate them in portable electronic devices [8,9].

The development of fibre-based supercapacitors has been mainly focused on novel electrode materials as they have a clear impact on the electrode performance [10,11]. In general, carbon nanomaterials (NM) – carbon nanotubes, graphene – have been widely used as electrodes in supercapacitors because of their large surface area and excellent electrochemical and electrical properties (that permits fast charge transport) [12,13] as well as their high mechanical strength and low density. However due to the limited capacitance values of carbon NM in addition to low production rates and high cost [14,15], most of the studies has focused on the preparation of multi-component composite fibres showing enhanced properties. For example, carbon-carbon composite fibres – CNT/graphene, CNT/mesoporous carbon particles – have better energy storage properties over their single component counteparts [8,16-18]. On the other hand, combining transition metal oxides (i.e. manganese, cobalt, nickel, vanadium or molybdenum oxides) as energy storage pseudocapacitive materials (high capacitance) with carbon nanomaterials (electrical conductivity) results in an excellent performance of electrodes and devices due to the synergistic effect between them [14]. Among the metal oxides under investigation, $MnO_2$ is one of the most promisings not only because of their high theoretical specific capacitance (up to 1370 F $g^{-1}$) but also because of their low cost and toxicity and high natural abundance [19,20]. Moreover, $MnO_2$ has the advantage that it can be synthesized with a variety of phases and morphologies with different specific surface areas and therefore different specific capacitances [21,22].

Examples of multimaterial fibres for electrodes have been proposed in earlier works. Xiao et al. [23] fabricated a $MnO_2$-cabon core-shell fibre after immersing the carbon fibre into a $KMnO_4/Na_2SO_4$ solution allowing the deposition of $MnO_2$ onto the carbon. Lu et al. also

obtained a core-shell fibre by electrodepositing $MnO_2$ onto a carbon nanotube fibre [24]. Or Gao et al. synthesized fibres based on carbon/Ni/carbon/Ni-Co double hydroxide layers. These multilayered fibres were obtained by very complicated procedures (more than 10 steps were required) [25]. Even though the multimaterial fibres showed good electrochemical performance, the core-shell structure limits the active material loading (up to day loading is restricted to <20wt.%) [26] as high thick shells reduce the accessible surface area and the bulk fibre core neither participates in the electrochemical charge/discharge process. Moreover, multistep synthesis procedures hinder the industrial scale preparation of the fibres and therefore practical engineering applications.

Recently the technique of wet-spinning has emerged as a promising method to develop fibre electrodes (e.g. PEDOT:PSS fibres, CNT and graphene fibres) for wearable electronics [27,28]. This technique, which allows the preparation of fibres with highly aligned nanomaterials, maintains the interesting properties of nanomaterials in the bulk and is a straightforward and scalable method to prepare flexible fibres in a continuous way [29,30].

Thus, in this work we are facing the electrode development from a two-perspective approach: selection of the different materials to accomplish a specific role in the fibre and wet-spinning as a suitable method for the macroscale assembly of the different nanomaterials into continuous fibres. On one hand, we have selected carbon black and carbon nanotubes as the electrically conductive network for fast electronic transport. Moreover, the different aspect ratio of both nanomaterials will help having a more open structure and therefore a higher surface access for the electrolyte. Birnessite $MnO_2$ nanotubes ($MnO_2$ NT) were incorporated into the fibre because of the enhanced specific capacitance of the birnessite phase together with the potential increase in the specific capacitance associated with nanotubes. Birnessite is a layered manganese oxide type (ideal formula $M_{0.5}MnO_2.xH_2O$, in this study M = K) with alkali metal ions and water of hydration between manganese oxide layers. The thinness of birnessite platelets allows access to almost all of the bulk $MnO_2$, meaning that close to 100% is at the surface, reason why birnessite has high specific capacitance [31-33]. Finally, chitosan was selected as the fibre matrix. Chitosan swells in water facilitating the ion transport within the fibre and therefore enhancing the electrochemical utilization of birnessite $MnO_2$ NT. On the other hand, the multimaterial fibres will be prepared by wet-spinning in a one step process. Therefore, the development of wet-spun multimaterial fibre electrodes for supercapacitors is still challenging.

The overall aim of the present work is the preparation of CB/CNT/$MnO_2$ NT fibres by a one-step wet-spinning process. First, CB, CNT and CB/CNT fibres will be studied and optimized to serve as the electrically conductive network and the current collector. The influence of the carbon nanomaterial employed and the dispersion conditions (pH, carbon NM concentration, surfactant/carbon NM ratio, CB/CNT concentration ratio) on the electrochemical properties of the fibres were studied. Subsequently the incorporation of birnessite nanotubes into the fibres was studied and optimized in order to improve fibre capacitance.

## 2. Experimental section

### 2.1. Materials

Carbon black and multiwall carbon nanotubes were purchased from Timcal Graphite & Carbon and Nanocyl, respectively. The characteristics of the carbon nanomaterials are found in Table 1. More detailed properties and characteristics can be found in the suppliers' technical data sheets and/or other published papers [34-37]. Chitosan powder, acetic acid ($CH_3COOH$) (99.8%), sodium dodecylbenzenesulfonate (SDBS), potassium chloride (KCl), phosphate buffered solution (PBS), hydrochloric acid (HCl), potassium permanganate ($KMnO_4$), potassium hydroxide (KOH) and 1-hexadecylamine ($CH_3(CH_2)_{15}NH_2$ were obtained from Sigma Aldrich.

Table 1. Summary of the CNT and carbon black characteristics supplied by the manufacturers.

| Carbon nanomaterial | Product name | Diameter (nm) | Length (μm) | Structure |
|---|---|---|---|---|
| Carbo nanotube | Nanocyl™ NC7000 | 9.5 | 1.5 | Amorphous |
| Carbon black | Super P Carbon black | 30-40 | --- | Amorphous |

Birnessite (potassium manganese oxide) nanotubes were synthesized through a templated hydrothermal route according to [32]. Briefly, $KMnO_4$ was added to KOH and stirred (15 min) before adding 1-hexadecylamine template. The slurry was transferred to a steel

autoclave and heated to 150ºC under autogenous pressure for 2 days with constant stirring before allowing the reaction to cool slowly to room temperature. The resultant material was thoroughly washed with water until pH=7 and refluxed in ethanol saturated with NaCl until removal of the hexadecylamine template.

### 2.2. Fabrication of multimaterial fibres and quasi-solid-state supercapacitor

Fibres were prepared by wet spinning. Briefly, wet spinning involves the dispersion of functional materials in a fluid, which is extruded through a spinneret into a coagulation bath, causing the fibre to precipitate and solidify. Four different dispersions were prepared containing: (i) CB, (ii) CNT, (iii) CB/CNT and (iv) CB/CNT/birnessite $MnO_2$ nanotubes. The concentration of the carbon nanomaterials was varied from 0.1 wt.% to 1 wt.% and the birnessite content from 0.1 wt.% to 0.4 wt.%. The concentration of the dispersant (sodium dodecylbenzenesulfonate (SDBS)) was altered according to the concentration of the functional nanomaterials to have SDBS/functional nanomaterials ratios between 0.5 and 2. The dispersions were sonicated in a horn sonicator for 30 min. The amplitude, power and frequency were 30 %, 500 W and 20 kHz respectively. The dispersions were injected through a needle (14 gauge) at an injection rate of 10 ml/min. The coagulation bath was an aqueous solution containing 0.5 wt.% chitosan and 0.5 wt.% acetic acid. The coagulation bath was rotated at 50 rpm in order to obtain continuous fibres. Fibres were rinsed in deionized water and then dried in air under tension.

The quasi-solid-state supercapacitors were prepared by coating two fibres with a gel electrolyte (PVA-$H_3PO_4$ 1:10), twisting them and drying at room temperature. Finally, the twisted fibres were coated again with the gel electrolyte. The electrochemical experiments were carried out connecting the two fibres with the electrical wires through metallic tweezers.

### 2.3. Equipment

A 5 ml syringe with a detachable needle (14 gauge) controlled by a syringe pump (KDS Scientific-100) was used to inject the dispersion to the coagulation bath. Fibre morphology was evaluated using a JEOL USA JSM-7100F Analytical Field Emission Scanning Electron Microscope (SEM). Samples were mounted on a stainless steel stub and connected to it using

silver paint. Energy dispersive spectroscopy (EDS) mapping was performed with the same scanning electron microscope. Raman spectroscopy of the fibres was measured using a Renishaw Systems 2000 Raman Microscope. A 514 nm green laser was used and the measurements performed at 50x magnification. Electrical conductivity was evaluated by the four-probe method, where a constant current was applied and the resultant voltage measured by a Keithley 2001 multimeter.

Electrochemical measurements (cyclic voltammetry (CV), galvanostatic charge-discharge (GCD)) were performed using a Gamry Reference 600 and eDAQ potentiostat EA161 and eDAQ e-recorder 410. A conventional three-electrode cell was used for CV and GCD, with conducting fibres as working electrode, Ag/AgCl/KCl (3M) reference electrode and platinum mesh counter electrode. The electrolytes employed were 0.01 mol $dm^{-3}$ PBS (phosphate buffered saline) and 0.1-0.5 mol $dm^{-3}$ KCl solutions for cyclic voltammetry and GCD experiments respectively. We selected neutral electrolytes because according to J.-G. Wang *et al.* [22] acidic or alkaline electrolytes show some disadvantages like dissolution of $MnO_2$ (in acid solutions) or the formation of the insulating $Mn(OH)_2$ in alkaline electrolytes, both phenomena hindering the applicability of the supercapacitors.

In all CV experiments, potential was scanned from 0 to 0.8 V with various scan rates (5-100 mV $s^{-1}$). For GCD, current density was varied from 0.5 to 10 A $g^{-1}$. The gravimetric capacitance of the fibres was calculated from GCD curves recorded in a three-electrode system using equation (1):

$$C = \frac{I\, t_d}{m\, \Delta V} \qquad (1)$$

where $I$, $t_d$, $m$ and $\Delta V$ are the applied current, the discharge time, the total mass of the fibre and the potential window, respectively.

On the other hand, when evaluating the gravimetric capacitance of the solid-state supercapacitor (2-electrode system), we can differentiate between cell capacitance ($C_{Cell}$) or electrode capacitance ($C_{elec}$). Cell capacitance is obtained using the same equation than before:

$$C = \frac{I\, t_d}{m\, \Delta V}$$

but in this case, *m* is the total mass of the two electrodes. Electrode capacitance is related with cell capacitance in the two-electrode configuration by the following equation [14]:

$$C_{elect} = 4\ C_{Cell}$$

The mass of each fibre was determined using a Sartorius MC5 microbalance.

## 3. Results and discussion

First, a range of optimisation studies were performed (variation of dispersion pH, carbon NM concentration, SDBS/ carbon NM concentration ratio and CB/CNT concentration ratio) to determine the best dispersion characteristics for fibre spinning. Table 2 summarises the conditions of pH and total carbon concentration conducive to spinning CB or CNT fibres. As it can be observed, for low CB concentration (0.1 wt.%) we only obtained fibres at pH=1.5, while no fibres were obtained at higher pH values. However, as the CB content increases to 0.5 wt.% fibres were obtained in the whole pH range studied. A further increase in the CB concentration led to the formation of aggregates in the dispersions independently of the pH. Therefore, these dispersions were discarded as aggregates would prevent fibres having a higher surface area for energy storage. On the other hand, CNT fibres were easily obtained for a CNT concentration of 0.1 wt.% and independently of the dispersion pH. Higher CNT contents led to the formation of aggregates and therefore these dispersions were also discarded. Based on these results, we selected 0.5 wt.% as the concentration to prepare CB fibres and 0.1 wt.% for CNT fibres. Finally, no great influence of SDBS concentration on spinnability was observed.

Table 2. Summary of the conditions, in terms of carbon nanomaterial concentration and pH, which allowed fibre formation.

| Carbon nanomaterial Concentration | Fibre | pH 1.5 | 2.5 | 3.5 | 4.5 |
|---|---|---|---|---|---|
| 0.1 wt.% | CB fibre | ✓ | X | X | X |
| 0.5 wt.% | CB fibre | ✓ | ✓ | ✓ | ✓ |
| 1 wt.% | CB fibre | Aggregates | Aggregates | Aggregates | Aggregates |
| 0.1 wt.% | CNT fibre | ✓ | ✓ | ✓ | ✓ |
| 0.5 wt.% | CNT fibre | Aggregates | Aggregates | Aggregates | Aggregates |
| 1 wt.% | CNT fibre | Aggregates | Aggregates | Aggregates | Aggregates |

Cyclic voltammetry was subsequently used to characterize the CB and CNT fibres prepared from 0.5 wt.% CB and 0.1 wt.% CNT dispersions respectively at the different pH values (1.5-4.5) and different SDBS/carbon NM ratios (0.5-2). Figure 1A,B shows the influence of the pH on the charge storage ability of the CB and CNT fibres. As we can observed for CB fibres, the lower the pH the more square the cyclic voltammetry, obtaining higher energy storage at pH 1.5. The repulsion between nanoparticles at more acidic pH's due to the adsorption of protons onto the carbon nanomaterials, favours more disperse solutions which translates into improved fibre properties. In contrast, cyclic voltammetries of CNT fibres are very similar in the pH range 1.5-3.5, starting losing the square shape at pH $\geq$ 4.5. Comparing CB and CNT fibres, the latter show higher current values (because the better electrical conductivity of CNT) and therefore, higher energy storage capacity.

After that, the influence of the SDBS content in the electrochemical performance of the wet-spun CB or CNT fibres was investigated, while maintaining the dispersion pH at 1.5. Thus, the SDBS/carbon nanomaterial ratio was modified from 0.5 to 2 in the dispersions containing only CB (0.5 wt.%) or CNT (0.1 wt.%). For CB (Fig. 1C), the increase in SDBS content up to 0.75 wt.% (SDBS/CB ratio = 1.5) enhances the current and the square shape of the cyclic voltammograms of CB fibres. Beyond this ratio, a further increase in SDBS content leads to a decrease in the electrochemical performance of the resulting fibre. The same trend is observed in CNT (Fig. 1D). As SDBS content increases, carbon nanomaterials are better

dispersed into the fibre resulting in a higher energy storage capacity; however, ratios higher than 1.5 reduces the capacitance as a result of a non-conductive wrapping of the carbon nanomaterials by SDBS. The optimum SDBS/carbon NM concentration ratio is 1.5 for both CB and CNT fibres. In summary, the optimum dispersions conditions leading to the best electrochemical performance are: (A) CB dispersions: 0.5 wt.% CB, pH 1.5 and SDBS /CB concentration ratio of 1.5 and (B) CNT-dispersions: 0.1 wt. % CNT, pH 1.5 and SDBS/CNT concentration ratio of 1.5.

We have also observed that replacement of some of the CNT content by CB enhanced the electrochemical performance. Thus, we prepared fibres containing different CB/CNT concentration ratios and studied their influence on the electrochemical properties of the fibres. The total concentration of the carbon nanomaterials in the dispersion was kept constant at 0.1 wt.% in order to avoid CNT agglomeration observed at higher concentrations. Within this total 0.1 wt.% the ratio of carbon black to CNT was varied preparing in total 7 different dispersions (Table 3). SEM micrographs of the as-spun fibre electrodes are shown in Fig. 2. SEM analyses of the cross-sections show the elliptical shape of the fibres with diameters in the range 30-35 μm independently of the fibre composition. Moreover, both nanomaterials can be clearly observed within the core of the fibre and surrounded by a chitosan polymer outer shell. Changing the dispersion composition results in fibres with different CB/CNT ratio inside the fibre. Thus, the higher the CNT content in the dispersion, the higher the CNT content in the fibre (Fig. 2E-H). Close inspection of the cross-sections allows observing a homogeneous distribution of the nanomaterials, suggesting they were well dispersed in solution. Moreover, CNT are oriented along the longitudinal axis of the fibre as a result of the wet-spinning process. Finally, rough surface corrugations were also observed parallel to the fibre axis.

Table 3. Composition of the dispersion used to wet-spun CB/CNT fibres and total percentage of the carbon nanomaterials into the dispersion.

| Fibre | CB content (wt.%) | CNT content (wt.%) | % CB | % CNT |
|---|---|---|---|---|
| I | 1.00 | 0.00 | 100% | 0% |
| II | 0.09 | 0.01 | 90% | 10% |
| III | 0.07 | 0.03 | 70% | 30% |

| | | | | |
|---|---|---|---|---|
| IV | 0.05 | 0.05 | 50% | 50% |
| V | 0.03 | 0.07 | 30% | 70% |
| VI | 0.01 | 0.09 | 10% | 90% |
| VII | 0.00 | 0.10 | 0% | 100% |

The electrical conductivity of the fibres was also measured by the four-point probe method. Figure 3 shows the electrical conductivity values for the single and composite fibres. Increasing the CNT content into the fibres increased the electrical conductivity from 4.4 S $cm^{-1}$ (100% CB) up to 14.7 S $cm^{-1}$ (10% CB/90% CNT). 100% CNT fibres showed a lower conductivity value (10.4 S $cm^{-1}$). This result suggests that carbon black particles act as an effective dispersant for CNTs creating a better electrically conductive network than in either CB or CNT fibres. Similar synergies have been observed previously for graphene oxide-CNT hybrid materials [38].

Figure 4A illustrates the evolution of the cyclic voltammograms of the CB/CNT composite fibres together with those for CB (Fibre I) and CNT fibres (Fibre VII). As it can be observed, increasing the CNT content in the composite fibres increased the current in the cyclic voltammetry, fibres III-VI having higher values than those recorded for the single one component fibres. A concurrent improvement in voltammogram shape towards the ideal rectangle is also observed. Carbon particles act as spacers to create gaps between the CNTs resulting in a higher surface area and therefore, better capacitance results. These results agree with the trend previously observed for the electrical conductivity of the fibres. Moreover, an incipient increase in the current around 0.8 V was observed for Fibre VI probably attributed to faradaic reactions.

GCD experiments in a three-electrode system were performed to quantify the capacitance of CB, CNT and CB/CNT composite fibres. First, we employed PBS as electrolyte; however due to the low capacitances measure we tried different common neutral electrolytes ($Na_2SO_4$, $(NH_4)_2SO_4$ and KCl). Among them, 0.5 M KCl led to obtain better capacitance values. GCD curves are almost symmetrical indicating a nearly ideal capacitive behaviour of all fibres (Fig. 4B). All fibre types show a voltage drop that is higher in CB (0.4 V) than in CNT (0.09 V) and CB/CNT fibres (0.04-0.07 V). This is expected since this voltage drop is associated with the internal resistance of the electrode, and CB fibres exhibit the lowest electrical conductivity. The voltage drop is dramatically reduced in CNT and even more in CB/CNT

fibres (with CNT contents higher than 70%), attributed to the higher electrical conductivity of CNTs and it is further increased by CB acting as an electrical contact between CNTs. The gravimetric capacitances calculated from the GCD curves are shown in Fig. 4C. The charge storage mechanism of these fibres is electrochemical double layer capacitance, which is based on the interfacial double-layer of high specific area carbons [38,39]. Replacing part of the CNT content with CB increased the capacitance of these fibres by up to a factor of 2.5 in Fibre VI. Two main effects can explain the improved electrochemical performance of the composite fibres: (i) mixing two nanomaterials with different aspect ratio results in fibres with more open structures, facilitated by CB dispersing the CNTs and yielding higher electrochemical surface area and (ii) the higher electrical conductivity of the composites fibres. GCD experiments over 10000 cycles were also performed to evaluate fibre life time (Fig. 4C). While capacitance retention of CB was reduced to 50%, those from CNT and CB/CNT fibres were 80% and 81-93% respectively. These results reflect a good electrochemical stability and a high degree of reversibility of the CB/CNT fibres.

As a proof of concept, a solid-state supercapacitor was prepared by intertwining two 10% CB/90% CNT fibres previously coated with a gel electrolyte (PVA-$H_3PO_4$). These fibres were chosen because they showed the best electrochemical performance among all the fibres. Figure 5A shows a picture of the supercapacitor (straight and bend positions) and a SEM image of the two electrodes coated with the gel electrolyte. The CV curves are symmetrical and almost rectangular in shape even at 100 mV $s^{-1}$ indicating good reversibility (Fig. 5B), and GCD curves show a triangular shape indicating good charge transport between the electrodes (Fig. 5C). A higher voltage drop (0.14V) than that measured for the 3-electrode system is observed which is attributed to the higher electrical resistivity of the gel electrolyte compared to the liquid electrolyte. The calculated cell and electrode capacitances of the device were 2.3 and 9.2 F $g^{-1}$ respectively. The electrode capacitance is slightly lower than in liquid electrolyte and is attributed to a reduced ionic mobility within the gel electrolyte. The electrochemical performance of the supercapacitor was not affected during mechanical bending; the CV and GCD curves for straight and bent positions are very nearly identical. Thus, 10% CB/90% CNT fibres are promising candidates for current collectors or active charge storage electrodes due to the good conductivity and the nano-network structure. Moreover, up to 10% CNT can be replaced by a less expensive material like CB (approx. 1 euro $kg^{-1}$) [20] leading to a reduction in the total cost of the supercapacitor. However, the

capacitance values and coulombic efficiency (around 50%) still remain low in comparison to other reported fibres [40,41].

In order to enhance the electrochemical performance, fibres were modified by incorporating birnessite-type manganese dioxide nanotubes. On one hand, $MnO_2$ is one of the most promising pseudocapacitive materials with high theoretical specific capacitance (1370 F $g^{-1}$), high natural abundance, low toxicity and low cost [42,43]. On the other hand, some birnessite $MnO_2$ materials have shown high specific capacitances at a relatively low specific surface area. This is a result of the thinness of birnessite platelets allowing access to almost all of the bulk $MnO_2$, effectively meaning that close to 100% is at the surface [31]. However, the poor electrical conductivity of $MnO_2$ could hinder its use [42,43]. Therefore, in this work we have incorporated birnessite nanotubes into the previously developed fibres in order to improve their electrochemical performance. While CB and CNT will confer electrical conductivity to the composite fibre, $MnO_2$ nanotubes will enhance fibre capacitance because the high energy storage capacity of the birnessite phase previously mentioned together with the potential increase in capacitance associated with nanotubes.

Birnessite $MnO_2$ nanotubes were synthesized according to [32]. Initially, 0.1 wt.% $MnO_2$ NT were added to the previously optimized CB/CNT dispersion resulting in: 0.01wt.% CB, 0.09 wt.% CNT, 0.1 wt.% $MnO_2$ NT, pH = 1.5, SDBS/(CB-CNT-$MnO_2$ NT) ratio = 1.5. We found this solution was not spinnable probably due to the instability of $MnO_2$ at pH=1.5 [44]. However, we were able to synthesise fibres from dispersions with pH in the range from 2.5 to 6.5. Figure 6 shows SEM images of fibre cross-sections and fibre surface after $MnO_2$ nanotubes incorporation. It is clear from the images that the $MnO_2$ nanotubes are incorporated into the fibre core together with CB and CNT and surrounded by chitosan shell. The arrows and the dashed circle in Fig. 6B point towards the different nanomaterials. On the other hand, no noticeable differences are observed in the fibre surface after $MnO_2$ NT incorporation, observing corrugation as in CB/CNT fibres.

The spatial distribution of the C, Mn and O in the fibre cross-sections was analysed using energy dispersive spectroscopy (EDS) coupled to SEM (Fig. 7A). It is clear from the elemental mapping that the fibres prepared from birnessite-containing dispersions have manganese in addition to carbon from the carbon nanomaterials and the chitosan shell. An homogeneous distribution of the carbon nanomaterials and $MnO_2$ NT is inferred from EDS mapping images.

Raman spectroscopy was useful to univocally detect the presence of the different nanomaterials into the fibre. The Raman spectra of CB/CNT and CB/CNT/$MnO_2$ NT fibres are seen in Fig. 7B. The CB/CNT fibre exhibited two strong peaks at 1340 $cm^{-1}$ and 1570 $cm^{-1}$ attributed to the D and G bands of carbon-based materials respectively (Fig. 7B, curve a). After the incorporation of the $MnO_2$ nanotubes, several peaks appeared in the 200-900 $cm^{-1}$ range, region where manganese oxide peaks are expected (Fig. 7B, curve b). This region is dominated by peaks at 643, 584 and 481 $cm^{-1}$ which are assigned to the stretching mode of $MnO_6$ octahedra [45,46]. These results are consistent with the presence of birnessite $MnO_2$ and are in agreement with previous reports [32,47]. We do not observe peaks corresponding to chitosan as Raman signal is much lower than for carbon nanomaterials and $MnO_2$ nanotubes.

To evaluate the electrochemical performance of the birnessite $MnO_2$-containing fibres prepared from dispersions containing 0.1 wt.% $MnO_2$ NT at different pH's, we first performed galvanostatic charge-discharge measurements in a three-electrode system. As it can be observed in figure 8A, fibre capacitance increases as the dispersion pH increases, obtaining the highest capacitance value at pH=5.5. No great differences are observed when the pH is increased to 6.5. This increase in capacitance from pH = 2.5 to 5.5 may be attributed to the higher contribution of $MnO_2$ because of the higher stability in less acid media. Capacitance is slightly reduced at higher pH probably because of the lower capacitance observed for carbon nanomaterials at pH $\geq$ 4.5. Among the different pH's, 5.5 seems the most effective in increasing the pseudo-capacitance of the electrode. A capacitance value of 50 F $g^{-1}$ was obtained representing a 5 time increase in the energy storage capacity of the CB/CNT/$MnO_2$ NT fibres. On the other hand, the GCD curves (Fig. 8B) for the CB/CNT/$MnO_2$ NT fibres show a voltage drop (0.1 V) that is slightly higher than those obtained for the CB/CNT fibres because of the low conductivity of $MnO_2$ nanotubes. Moreover, an asymmetry between the charge and discharge curves is observed which is attributed to the presence of the pseudocapacitive $MnO_2$ according to the literature [48,49]. All GCD curves showed asymmetry independently of the dispersion pH. The coulombic efficiency in the CB/CNT/$MnO_2$ NT electrodes is higher (70%) than that found for the carbon-based supercapacitor device and similar to those published [49,50].

These results may seem contradictory to the previously optimized experiments for CB/CNT fibres where the optimum pH was 1.5 to get the best capacitance value. However, the reduction in the CB/CNT/$MnO_2$ NT fibre capacitance because of the increase of pH to 5.5 is

not very relevant. According to the results previously shown, CB has the highest reduction in capacitance when pH increased from 1.5 to 5.5 compared to CNT. However, CB represents only 2-5 % (depending on the $MnO_2$ concentration range) of the total content of the functional materials in the fibres. This small amount does not significantly affect the total capacitance of the fibre. As a result, the fibres containing $MnO_2$ showed the best capacitance values with a 25-fold increment regarding CB/CNT fibres. Based on these results, we would like to remark that the fibre functional nanomaterials have different roles. Meanwhile carbon nanomaterials confer electrical conductivity to the fibre, birnessite $MnO_2$ is the energy storage material. At this point, we checked that the electrical conductivity of CB/CNT fibres did not change with the dispersion pH in the range 1.5-5.5, as it could hinder the electrochemical properties of the composite fibre electrode.

Fig. 8C,D shows the CV curves at a scan rate of 100 mV $s^{-1}$ from 0.0 to 0.8 V *vs* Ag/AgCl reference electrode at different pH values. In all the pH range studied, non-quasi rectangular and symmetric CV curves without redox peaks are recorded indicating typical pseudocapacitive behaviour of birnessite $MnO_2$ nanotubes and good reversibility during the energy storage process [5]. Moreover, the deviation from the ideal CV curves is observed, the curves becoming less ideal as the pH decreases (Fig. 8C) because some parts of the $MnO_2$ NT can be dissolved in acidic dispersions causing the loss of the active material and therefore lower capacitance [44,51]. Thus, the enclosed areas of CV curves are smaller at more acid pH. On the other hand, when the scan rate was increased the cyclic voltammetries were also less ideal and deviated from the horizontal (Fig. 8D). The supercapacitive behaviour of birnessite is dependent on the electrolyte ions insertion/deinsertion into the fibre which is a diffusion-controlled process. At low scan rates the diffusion process is able to take place into almost all the available pores. However, at higher scan rates this interaction is decreased as a lower number of ions approach the electrode surface with very little interaction, causing a deviation from the ideal rectangular shape and also angling of the CV curve away from the horizontal [52,53]. The lower electrical resistance of CB/CNT/$MnO_2$ NT fibres compared to the carbon-based fibres could also contribute to the deviation from the rectangular shape. It is also worthy to mention that all the curves are symmetric indicating good reversibility even at the higher scan rates.

After that, we modified the content of birnessite-$MnO_2$ nanotubes into the fibres. To do so, we prepared dispersions containing $MnO_2$ NT in the range 0.2 to 0.4% (keeping the carbon nanomaterials content at 0.1 wt.%) at pH = 5.5. SEM images of the cross-sections reveal the

higher amount of $MnO_2$ NT into the fibre as the content into the dispersion was increased. Rough corrugated surfaces were again obtained. We first used galvanostatic charge-discharge measurements to assess the electrochemical performance of the fibres as electrodes for energy storage devices. Figure 9A shows that the capacitance peaked at 0.2 wt.% $MnO_2$ NT concentration. A capacitance value of around 247 F $g^{-1}$ (considering the total mass of the fibre) was obtained, representing a 25-fold increment regarding CB/CNT based fibres. The reversible redox reactions occurring between the $MnO_2$ on the electrode and the ions in the electrolyte allow Faradaic charge transfer to take place. The mechanism is based on the adsorption/desorption of alkali metal cations into/from $MnO_2$:

$$(MnO_2)_{surface} + M^+ + e^- \rightleftharpoons (MnO_2^-M^+)_{surface}$$

with a simultaneous redox reaction between Mn(III) and Mn(IV) [22]. Therefore, the observed increase in capacitance is attributed to both the high specific capacitance of the birnessite phase and its tubular morphology with higher surface area. Moreover, the swelling of the chitosan shell and the good electrical conductivity of the CB/CNT network facilitate the electron transport within the fibre and enhance the electrochemical utilization of $MnO_2$. However, higher contents of $MnO_2$ nanotubes lead to a decrease in the specific capacitance due to the low electrically conductive nature of manganese oxides. Again, differences in the symmetry of the charge discharge curves were observed and due to the presence of the pseudocapacitive nature of birnessite $MnO_2$.

On the other hand, the CV curves of the fibres containing different amounts of $MnO_2$ NT are shown in Fig. 9B. Again, cyclic voltammograms are non-quasi rectangular and symmetric indicating the presence of a pseudocapacitive material and a good reversibility of the ions insertion/deinsertion process. On the other hand, the areas under the curves for the different $MnO_2$ NT compositions are ordered as follow: 0.2wt.% > 0.3 wt.% > 0.1 wt.% > 0.4 wt.%, which agrees with the capacitance values obtained by charge/discharge measurements.

GCD experiments were also carried out at various current densities for the fibre showing the highest specific capacitance (Fig. 9C). An initial drop in the specific capacitance was observed as the current density was increased to 2 A $g^{-1}$, becoming less significant at higher current densities. At such high current densities, the ions are not allowed to diffuse and being able to access as much of the pore structure, resulting in a lower electrochemical surface area and hence lower capacitance. However, even when the current was increased by a factor of

20, around 60% of the initial capacitance was maintained, indicating a good rate capability of the fibres. It is important to highlight that a specific capacitance of almost 250 F $g^{-1}$ was obtained at low discharge current density (0.5 A $g^{-1}$). This value is particularly high for fibre-based electrodes pointing towards a promising supercapacitor electrode material.

Finally, cycle life time was performed as it is another key factor for practical applications. An initial drop in specific capacitance was observed for the first 50 cycles (Fig. 9D) after which time it reaches a plateau, exhibiting a capacitance retention value of around 86% over 5000 cycles. This means that the fibres show excellent cyclability together with high capacitance values. Both are similar to those published for composite fibre electrodes obtained under more complex procedures.

From all these results, we can confirm that all the materials selected show a specific role within the fibre: (i) CB and CNT form an electrically conductive network resulting in a effective electron pathway for the full utilization of $MnO_2$ NT, (ii) chitosan polymer, apart from being the matrix of the composite fibre, swells in the aqueous electrolyte favoring its access towards the manganese dioxide surface, (iii) birnessite $MnO_2$ nanotubes show high specific capacitance at a low specific surface area due to the thinness of birnessite platelets allowing access to almost all of the bulk $MnO_2$. Therefore, an effective new strategy – wet-spinning of composite fibres in a single step – for electrode fabrication has been successfully tested.

## 4. Conclusions

In summary, we have successfully wet-spun fibres based on carbon nanomaterials and birnessite $MnO_2$ nanotubes with high electrochemical performance for supercapacitor applications. All the materials were meticulously selected according to their properties. The type of carbon nanomaterial and the dispersion conditions (pH, nanomaterial concentration and dispersant/carbon nanomaterial ratio) greatly affect the electrochemical performance of the fibres. Moreover, the mixture of 10% CB and 90% CNT leads to fibres with improved electrochemical characteristics because a better electrical connection between CNT exists due to the bridging role of CB. These fibres were assembled into a solid-state supercapacitor showing good electrochemical performance, in both straight and bent states. The incorporation of $MnO_2$ NT into the electrically conductive and swellable CB/CNT fibres

improved the capacitance by 25 times due to the high specific capacitance of the birnessite phase and its tubular morphology with higher surface area. Moreover, CB/CNT/$MnO_2$ NT showed good long term cyclability (87%). Thus, the selection of the materials and the technique are very important for real technological applications.

**Acknowledgements**

We acknowledge financial support from Engineering and Physical Sciences Research Council (EPSRC, UK) for the project *Advanced fibre-based energy storage for wearable applications* (Project number EP/K035002/1).

**References**

[1] C. Meng, C. Liu, L. Chen, C. Hu, S. Fan, Highly flexible and all-solid state paper like polymer supercapacitors, Nano Lett. 10(10) (2010) 4025-4031.

[2] M. Kaempgen, C.K. Chan, J. Ma, Y. Cui, G. Gruner, Printable thin film supercapacitors using single-walled carbon nanotubes, Nano Lett. 9(5) (2009) 1872-1876.

[3] Z. Weng, Y. Su, D.-W. Wang, F. Li, J. Du, H.-M. Cheng, Graphene cellulose paper flexible supercapacitors, Adv. Energy Mater. 1 (2011) 917-922.

[4] J. Garcia-Torres, C. Crean, E. Valles, Mater. Des. 141(5) (2018) 9-16.

[5] P. Simon, Y. Gogotsi, Materials for electrochemical capacitors, Nat. Mater. 7 (2008) 845-854.

[6] X. Yang, C. Cheng, Y. Wang, L. Qiu, D. Li, Liquid-mediated dense integration of graphene materials for compact capacitive energy storage, Science 341(6145) (2013) 534-537.

[7] P.J. Hall, M. Mirzaeian, S.I. Fletcher, F.B. Sillars, A.J.R. Rennie, G.O. Shitta-Bey, G. Wilson, A. Cruden, R. Carter, Energy storage in electrochemical capacitors: designing functional materials to improve performance. Energ. Environ. Sci. 3 (2010) 1238-1251.

[8] L. Kou, T. Huang, B. Zheng, Y. Han, X. Zhao, K. Gopalsamy, H. Sun, C. Gao, Coaxial wet-spun yarn supercapacitors for high energy density and safe wearable electronics, Nat. Comm. 5 (2014) 3754-3763.

[9] J.A. Lee, M.K. Shin, S.H. Kim, H.U. Cho, G.M. Spinks, G.G. Wallace, M.D. Lima, X. Lepró, M.E. Kozlov, R.H. Baughman, Ultrafast charge and discharge biscrolled yarn supercapacitors for textiles and microdevices, Nat. Comm. 4 (2013) 1970-1977.

[10] D.P. Dubal, N.R. Chodankar, D.-H. Kim, P. Gomez-Romero, Towards flexible solid-state supercapacitors for smart and wearable electronics, Chem. Soc. Rev. 47 (2018) 2065-2129.

[11] F. Meng, Q. Li, L. Zheng, Flexible fiber-shaped supercapacitors: Design, fabrication, and multi-functionalities, Energy Storage Mater. 8 (2017) 85-109.

[12] L.T. Linh, M.H. Ervin, H. Qiu, B.E. Fuchs, W.Y. Lee, Graphene supercapacitor electrodes fabricated by inkjet printing and thermal reduction of graphene oxide, Electrochem. Comm. 13 (2011) 355-358.

[13] T. Chen, L. Dai, Flexible supercapacitors based on carbon nanomaterials, J. Mater. Chem A 2 (2014) 10756-10775.

[14] D. Yu, Q. Qian, L. Wei, W. Jiang, K. Goh, J. Wei, J. Zhang, Y. Chen, Emergence of fiber supercapacitors, Chem. Soc. Rev. 44 (2015) 647-662

[15] L. Dai, D.W. Chang, J.B. Baek, W. Lu, Carbon nanomaterials for advanced energy conversion and storage, Small, 8 (2012) 1130-1166.

[16] Y. Ma, P. Li, J.W. Sedloff, X. Zhang, H. Zhang, J. Liu, Conductive graphene fibres for wire-shaped supercapacitors strengthened by unfunctionalized few-walled carbon nanotubes, ACS Nano 9(2) (2015) 1352-1359

[17] J. Ren, W. Bai, G. Guan, Y. Zhang, H. Peng, Flexible and weaveable capacitor wire based on a carbon nanocomposite fiber, Adv. Mater. 25 (2013) 5965-5970.

[18] J. Foroughi, G.M. Spinks, D. Antiohos, A. Mirabedini, A. Gambhir, G.G. Wallace, S.R. Ghorbani, G. Peleckis, M.E. Kozlov, M.D. Lima, R.H. Baughman, Highly Conductive Carbon Nanotube-Graphene Hybrid Yarn, Adv. Funct. Mater. 24 (2014) 5859-5865.

[19] A.E. Fischer, K.A. Pettigrew, D.R. Rolison, R.M. Stroud, J.W. Long, Incorporation of homogeneous, nanoscale, $MnO_2$ within ultraporous carbon structures via self-limiting electroless deposition: implications for electrochemical capacitors, Nano Lett. 7(2) (2007) 281-286

[20] D. Talarico, F. Arduini, A. Constantino, M. Del Carlo, D. Compagnone, D. Moscone, G. Palleschi, Carbon black as successful screen-printed electrode modifier for phenolic compound detection, Electrochem. Comm. 60 (2015) 78-82.

[21] W. Wei, X. Cui, W. Chen, D.G. Ivey, Manganese oxide-based materials as electrochemical supercapacitor electrodes, Chem. Soc. Rev. 40 (2011) 1697-1721.

[22] J.-G. Wang, F. Kang, B. Wei, Engineering of $MnO_2$-based nanocomposites for high-performance supercapacitors, Progr. Mater. Sci. 74 (2015) 51-124.

[23] X. Xiao, T. Li, P. Yang, Y. Gao, H. Jin, W. Ni, W. Zhan, X. Zhang, Y. Cao, J. Zhong, L. Gong, W.-C. Yen, W. Mai, J. Chen, K. Huo, Y.-L. C., Z. L. Wang, J. Zhou, Fiber-Based All-Solid-State Flexible Supercapacitors for Self-Powered Systems, ACS Nano 6 (10) (2012) 9200-9206.

[24] Z. Lu, Y. Chao, Y. Ge, J. Foroughi, Y. Zhao, C. Wang, H. Long, G.G. Wallace, High-performance hybrid carbon nanotube fibers for wearable energy storage, Nanoscale 9 (2017) 9 5063-5071.

[25] L. Gao, J.A. Surjadi, K. Cao, H. Zhang, P. Li, S. Xu, C. jiang, J. song, D. Sun, Y. Lu, ACS Appl. Mater. Interf. 9 (2017) 9 5409-5418.

[26] C. Choi, K. M. Kim, K. J. Kim, X. Lepro, G. M. Spinks, R. H. Baughman, S. J. Kim, Improvement of system capacitance via weavable superelastic biscrolled yarn supercapacitors, Nat. Comm. 7 (2016) 13811-13818.

[27] R. Jalili, J.M. Razal, P.C. Innis, G.G. Wallace, One-step wet-spinning process of poly(3,4-ethylenedioxythiophene):Poly(styrenesulfonate) fibers and the origin of higher electrical conductivity, Adv. Funct. Mater. 21 (2011) 3363-3370.

[28] R. Jalili, S.H. Aboutalebi, D. Esrafilzadeh, K. Konstantinov, J.M. Razal, S.E. Moulton, G.G. Wallace, Formation and processability of liquid crystalline dispersions of graphene oxide, Mater. Horiz. 1 (2014) 87-91.

[29] X. Sun, T. Chen, Z. Yang, H. Peng, The alignment of carbon nanotubes: An effective route to extend their excellent properties to macroscopi scale, Acc. Chem. Res. 46(2) (2013) 539-549.

[30] Z. Xu, C. Gao, Graphene in macroscopic order: liquid crystals and wet-spun fibers, Acc. Chem. Res. 47(4) (2014) 1267-1276.

[31] T. Brousse, M. Toupin, R. Dugas, L. Athouel, O. Crosnier, D.J. Belanger, Crystalline $MnO_2$ as Possible Alternatives to Amorphous Compounds in Electrochemical Supercapacitors, J. Electrochem. Soc. 153 (2006) A2171-A2180.

[32] A.J. Roberts, R.C.T. Slade, Birnessite nanotubes for electrochemical supercapacitor electrodes, Energy Environm. Sci. 4 (2011) 2813-2817.

[33] A. Cormie, A. Cross, A.F. Hollenkamp, S.C. Donne, Cycle stability of birnessite manganese dioxide for electrochemical capacitors, Electrochim. Acta, 55 (2010) 7470-7478.

[34] S.A. Nanocyl, NANOCYL™ NC7000 series – Product Datasheet – Thin Multi-Wall Carbon Nanotubes (12th July 2016 – V08) (http://www.nanocyl.com/wp-content/uploads/2016/07/DM-TI-02-TDS-NC7000-V08.pdf) (last accessed: 4th July 2018).

[35] R.M. Gnanamuthu, C.W. Lee, Electrochemical properties of Super P carbon black as an anode active material for lithium-ion batteries, Mater. Chem. Phys. 130 (2011) 831-834.

[36] V. Palomares, A. Goñi, I. Gil de Muro, I. de Meatza, M. Bengoechea, I. Cantero, T. Rojo, Conductive additive content balance in Li-ion battery cathodes: Commercial carbon blacks vs. *in situ* carbon from LiFePO4/C composites, J. Power. Sources 195 (2010) 7661-7668.

[37] C.M. White, R. Banks, I. Hamerton, J.F. Watts, Characterisation of commercially CVD grown multi-walled carbon nanotubes for paint applications, Progr. Org. Coat. 90 (2016) 44-53.

[38] L. Qiu, X. Yang, X. Gou, W. Yang, Z.F. Ma, G.G. Wallace, D. Li, Dispersing Carbon Nanotubes with Graphene Oxide in Water and Synergistic Effects between Graphene Derivatives, Chemistry-A European Journal 16(35) (2010) 10653-10658.

[39] G. Wang, L. Zhang, J. Zhang, A review of electrode materials for electrochemical supercapacitors, Chem. Soc. Rev. 41 (2012) 797-828.

[40] S.T. Senthilkumar, Y. Wang, H. Huang, Advances and prospects of fiber supercapacitors, J. Mater. Chem. A 3 (2015) 20863-20879.

[41] L. Dong, C. Xu, Y. Li, Z.-H. Huang, F. Kang, Q.-H. Yang, X. Zhao, Flexible electrodes and supercapacitors for wearable energy storage: a review by category, J. Mater. Chem. A 4 (2016) 4659-4685.

[42] M. Toupin, T. Brousse, D. Belanger, Charge storage mechanism of $MnO_2$ electrode used in aqueous electrochemical capacitor, Chem. Mater. 16(16) (2004) 3184-3190.

[43] J. Garcia-Torres, C. Crean, Multilayered Flexible Fibers with High Performance for Wearable Supercapacitor Applications, Adv. Sust. Syst. 2(2) (2018) 1700143-1700152

[44] C. Tanggarnjanavalukul, N. Phattharasupakun, J. Wutthiprom, P. Kidkhunthod, M. Sawangphruk, Charge storage mechanisms of birnessite-type $MnO_2$ nanosheets in $Na_2SO_4$ electrolytes with different pH values: *In situ* electrochemical X-ray absorption spectroscopy investigation, Electrochim. Acta 273 (2018) 17-25.

[45] R. Baddour-Hadjean, J.-P Pereira-Ramos, Raman microspectrometry applied to the study of electrode materials for lithium batteries, Chem. Rev. 110 (2010) 1278-1319.

[46] C.M. Julien, M. Massot, C. Poinsignon, Lattice vibrations of manganese oxides. Part I. Periodic structures, Spectrochim. Acta Part A 60 (2004) 689–700.

[47] J. Zhang, X. Zhao, Z. Huang, T. Xu, Q. Zhang, High-performance all-solid-state supercapacitors based on manganese dioxide/carbon fibres, Carbon, 107 (2016) 844-851.

[48] X. Li and B. Wei, Facile synthesis and super capacitive behaviour of SWNT/$MnO_2$ hybrid films, Nano Energy 1 (2012) 479-487.

[49] H. Huang, W. Zhang, Y. Fu, X. Wang, Controlled growth of nanostructured $MnO_2$ on carbon nanotubes for high-performance electrochemical capacitors, Electrochim. Acta 152 (2015) 480-488.

[50] J. Tao, N. Liu, W. Ma, L. Ding, L. Li, J. Su, Y. Gao, Solid-state high performance flexible supercapacitors based on polypyrrole-MnO2-carbon fiber hybrid structure, Sci. Reports 3 (2013) 2286-2292.

[51] Z. Liu, R. Ma, Y. Ebina, K. Takada, T. Sasaki, Synthesis and Delamination of Layered Manganese Oxide Nanobelts, Chem. Mater. 19 (2007) 6504-6512.

[52] Q. Wang, Z. Wen, J. Li, A Hybrid Supercapacitor Fabricated with a Carbon Nanotube Cathode and a $TiO_2$–B Nanowire Anode, Adv. Funct. Mater. 16 (2006) 2141-2146.

[53] M.W. Xu, L.B. Kong, W.J. Zhou, H.L. Li, Hydrothermal synthesis and pseudocapacitance properties of α-$MnO_2$ hollow spheres and hollow urchins, J. Phys. Chem. C 111 (2007) 19141-19147.

**Figure Captions**

Figure 1. Influence of pH and SDBS/carbon NM ratio on the cyclic voltammetry of carbon black (A,C) and carbon nanotube (B,D) fibres. Scan rate: 100 mV $s^{-1}$. Electrolyte: PBS 0.01 mol $dm^{-3}$.

Figure 2. Low and high magnified cross-section SEM images of CB/CNT fibres with different compositions: (A,E) 100% CB, (B,F) 70% CB/30% CNT, (C,G) 30% CB/70% CNT, (D,H) 100% CNT.

Figure 3. Variation of the electrical conductivity with fibre composition.

Figure 4. (A) Cyclic voltammetries (Scan rate: 100 mV $s^{-1}$. Electrolyte: PBS 0.01 mol $dm^{-3}$), (B) galvanostatic charge-discharge curves (Applied intensity: 0.5 A $g^{-1}$. Electrolyte: KCl 0.5 mol $dm^{-3}$ and (C) Variation of capacitance and capacitance retention with fibre composition.

Figure 5. Picture and SEM image of the solid-state supercapacitor using 10% CB/90% CNT fibres. Cyclic voltammograms and GCD curves of the solid-state supercapacitor while straight and bent.

Figure 6. SEM images of (A) surface and (B-D) cross-sections of CB/CNT/$MnO_2$ NT fibres.

Figure 7. (A) Cross-section SEM image and corresponding EDS mapping of carbon, manganese and oxygen for the CB/CNT/$MnO_2$ NT fibres. (B) Raman spectra of CB/CNT (curve a) and CB/CNT/$MnO_2$ NT (curve b) fibres.

Figure 8. (A) Variation of CB/CNT/$MnO_2$ NT fibre capacitance with dispersion pH. The content of $MnO_2$ NT in the dispersion is 0.1 wt.%. (B) Galvanostatic charge discharge curves for the same fibres at pH=5.5. Electrolyte: 0.5 mol $dm^{-3}$ KCl. Applied intensity: 0.5 A $g^{-1}$. (C) Cyclic voltammetries from the CB/CNT/$MnO_2$ NT fibres prepared at different dispersion pH's. Scan rate: 100 mV $s^{-1}$. Electrolyte: PBS 0.01 mol $dm^{-3}$. (D) Cyclic voltammetries from the CB/CNT/$MnO_2$ NT fibres (dispersion pH=5.5) at different scan rates. Electrolyte: PBS 0.01 mol $dm^{-3}$.

Figure 9. (A) Variation of CB/CNT/$MnO_2$ NT fibre capacitance with dispersion $MnO_2$ NT concentration. (B) Cyclic voltammetries from CB/CNT/$MnO_2$ NT fibres containing variable amounts of $MnO_2$ NT. Scan rate: 100 mV $s^{-1}$. Electrolyte: PBS 0.01 mol $dm^{-3}$. (C) Variation of capacitance with applied intensity and (D) Cycling stability performance of CB/CNT/$MnO_2$ NT fibres containing 0.2 wt.% $MnO_2$ NT over 5000 cycles. Electrolyte: 0.1 mol $dm^{-3}$ KCl. Applied intensity: 2 A $g^{-1}$.

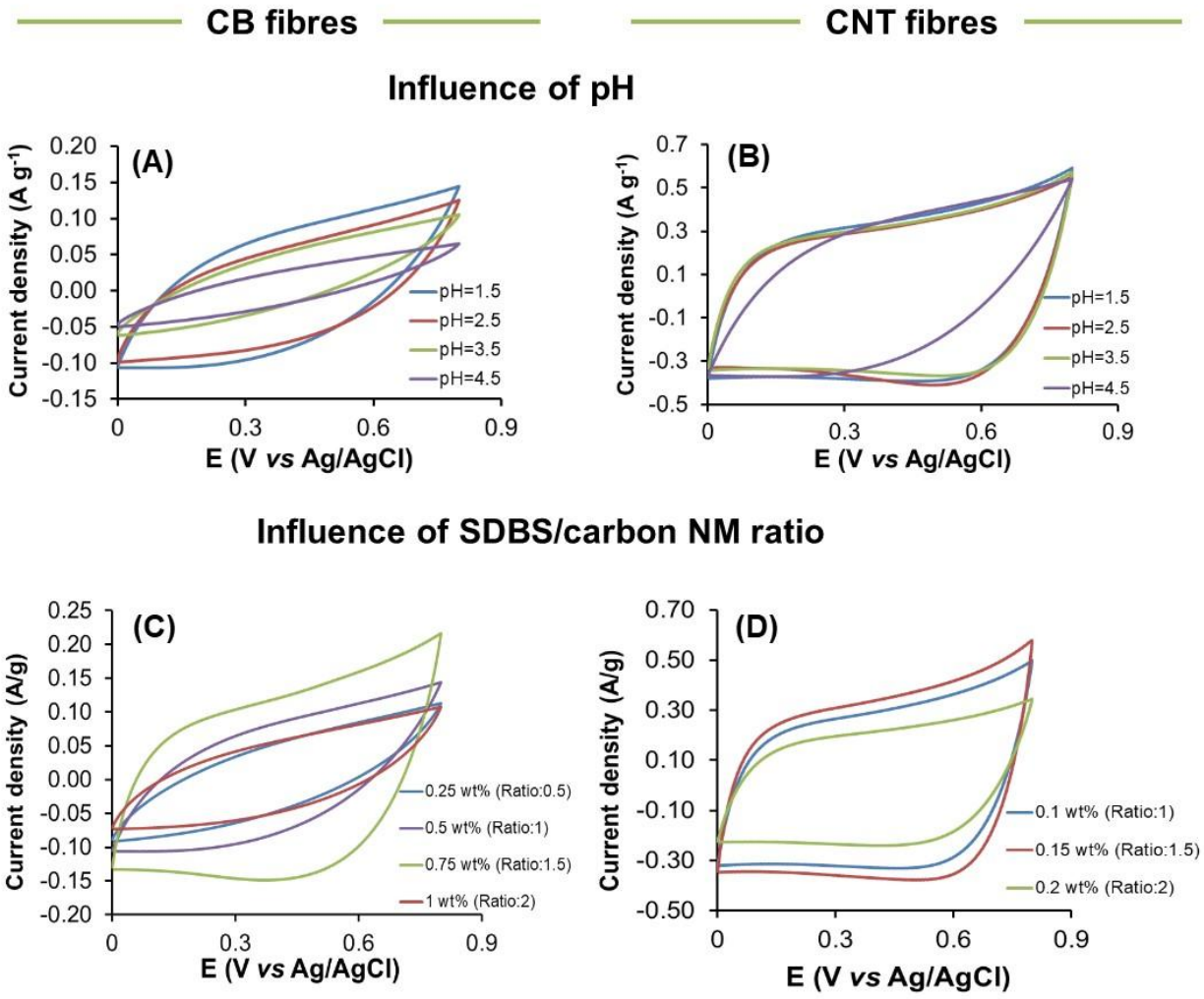
CB fibres
CNT fibres
Influence of pH
(A)
(B)
Current density (A g-1)
E (V vs Ag/AgCl)
pH=1.5
pH=2.5
pH=3.5
pH=4.5
Influence of SDBS/carbon NM ratio
(C)
(D)
Current density (A/g)
0.25 wt% (Ratio:0.5)
0.5 wt% (Ratio:1)
0.75 wt% (Ratio:1.5)
1 wt% (Ratio:2)
0.1 wt% (Ratio:1)
0.15 wt% (Ratio:1.5)
0.2 wt% (Ratio:2)

**Figure 1**

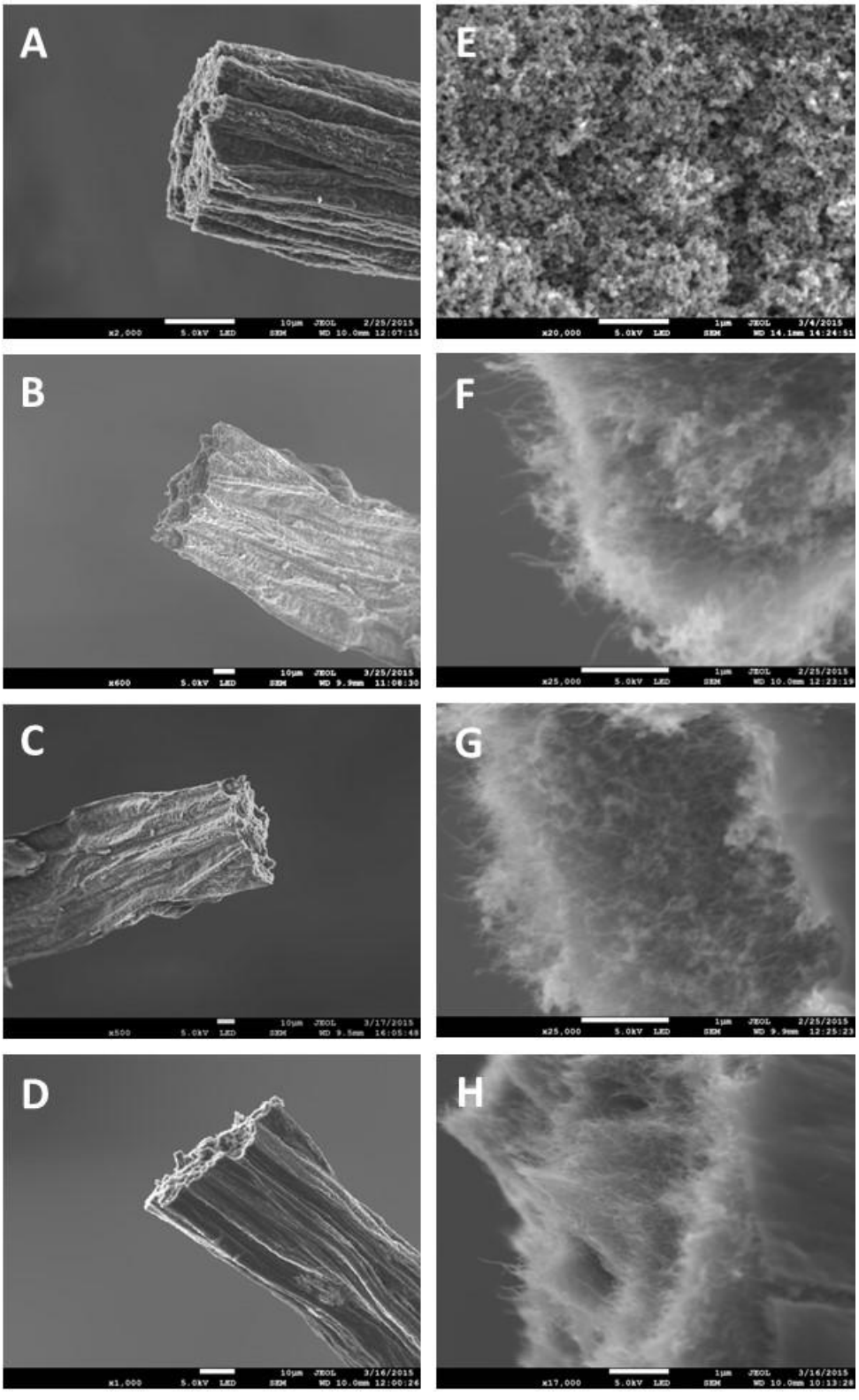


**Figure 2**

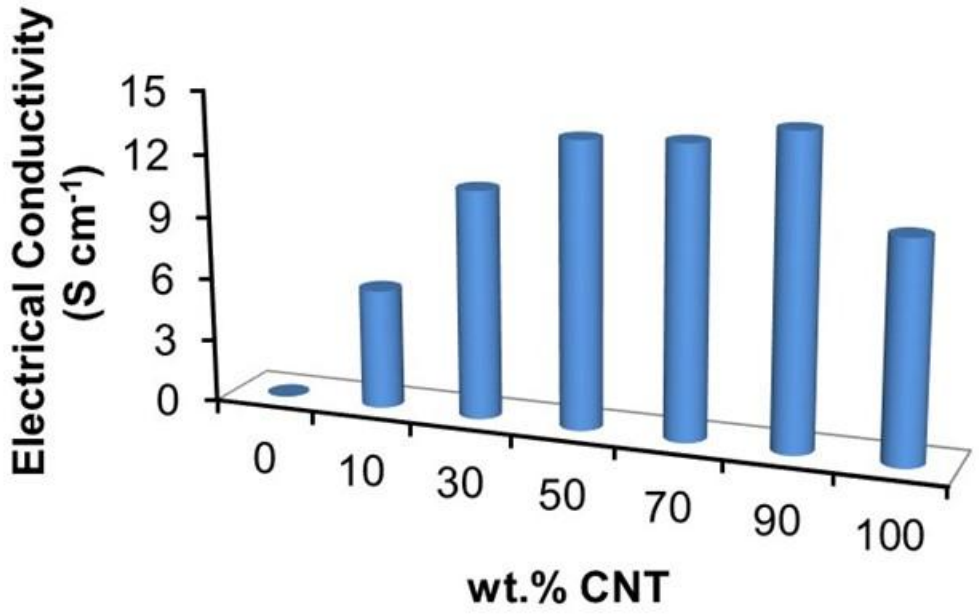
Electrical Conductivity
(S cm-1)
15
12
9
6
3
0
0
10
30
50
70
90
100
wt.% CNT

**Figure 3**

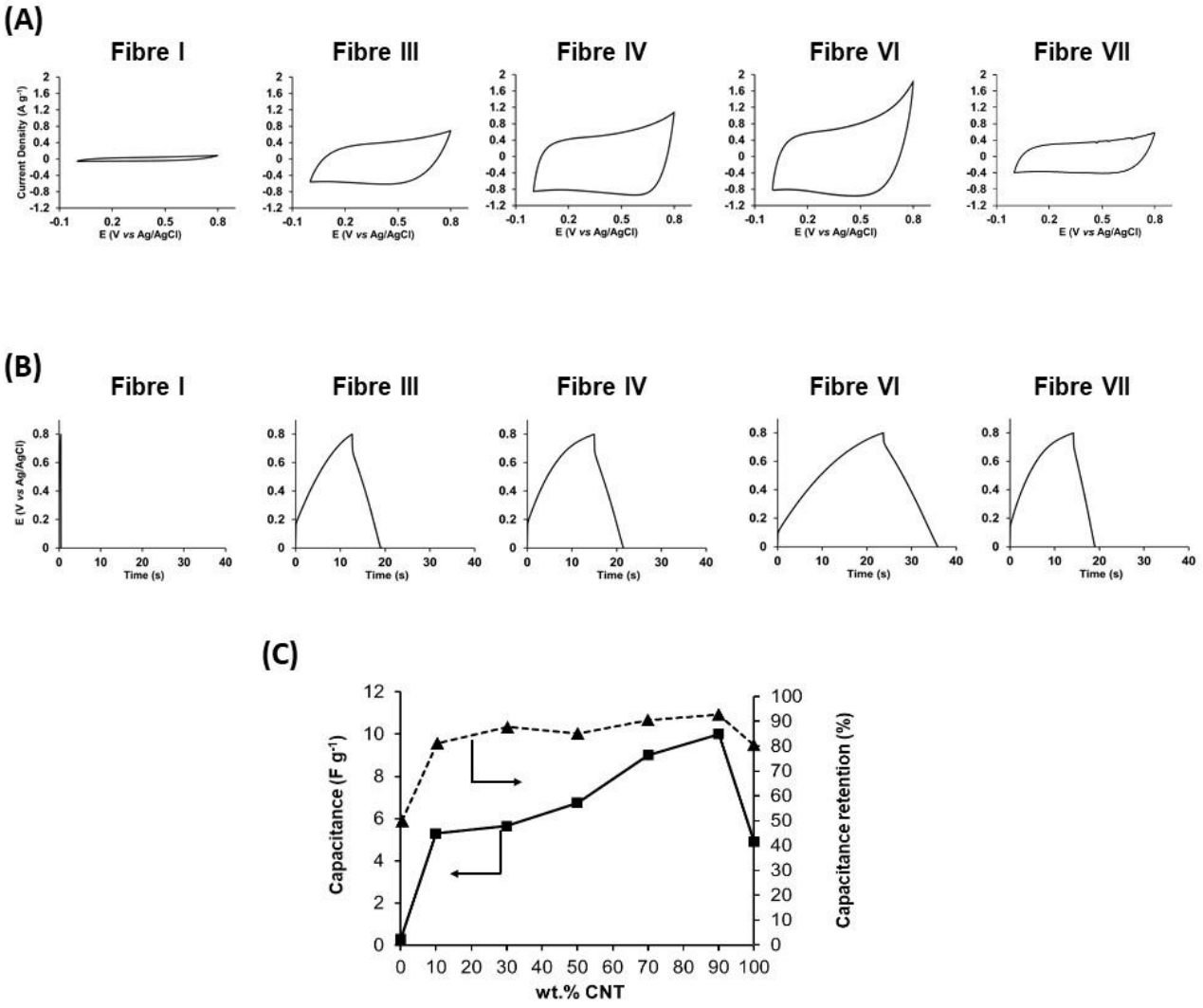
(A)
Fibre I
Fibre III
Fibre IV
Fibre VI
Fibre VII
Current Density (A g⁻¹)
E (V vs Ag/AgCl)
(B)
Fibre I
Fibre III
Fibre IV
Fibre VI
Fibre VII
E (V vs Ag/AgCl)
Time (s)
(C)
Capacitance (F g⁻¹)
Capacitance retention (%)
wt.% CNT

**Figure 4**

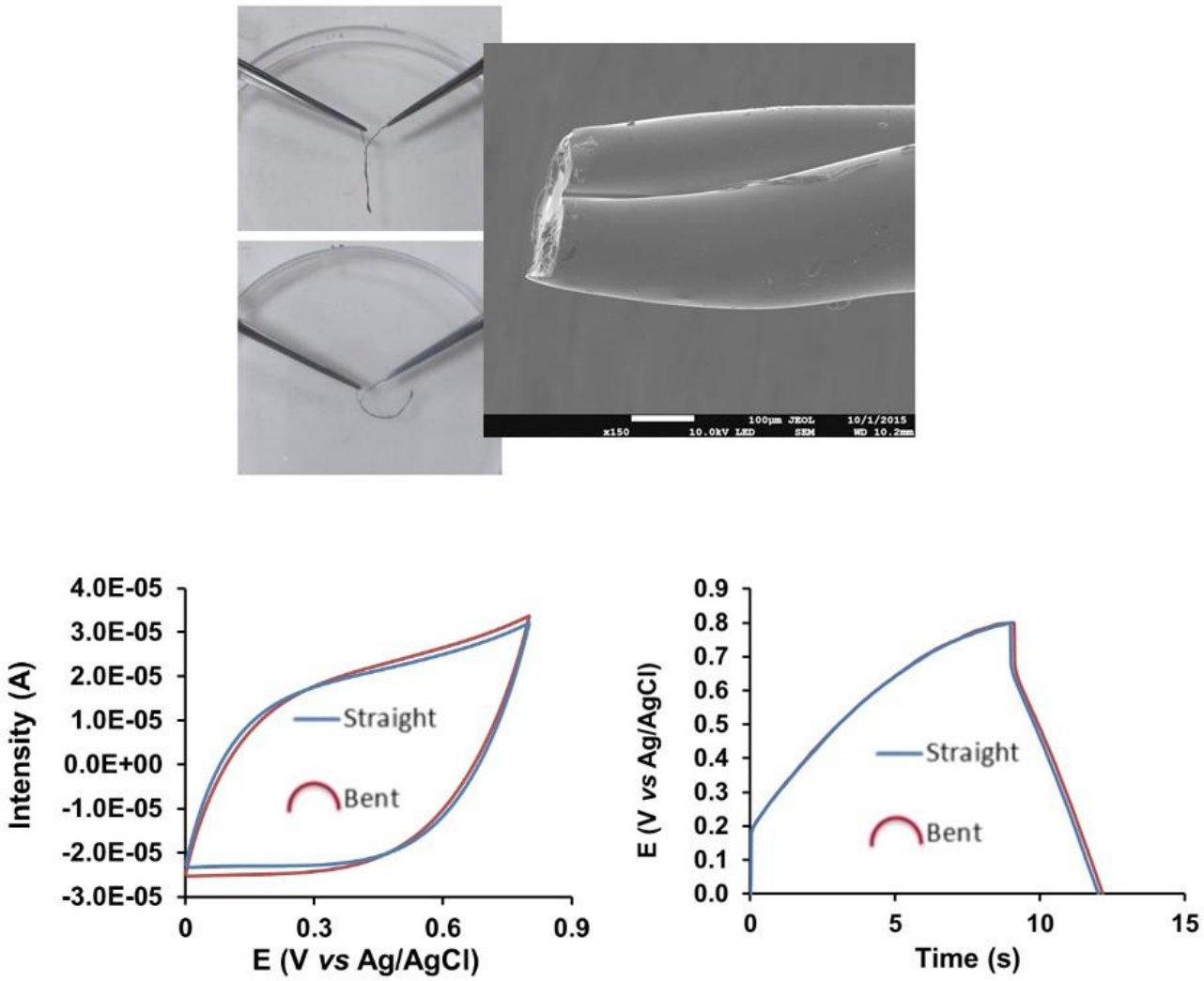
100µm JEOL 10/1/2015
x150 10.0kV LED SEM WD 10.2mm
4.0E-05
3.0E-05
2.0E-05
1.0E-05
0.0E+00
-1.0E-05
-2.0E-05
-3.0E-05
Intensity (A)
Straight
Bent
0
0.3
0.6
0.9
E (V vs Ag/AgCl)
0.9
0.8
0.7
0.6
0.5
0.4
0.3
0.2
0.1
0.0
E (V vs Ag/AgCl)
Straight
Bent
0
5
10
15
Time (s)

**Figure 5**

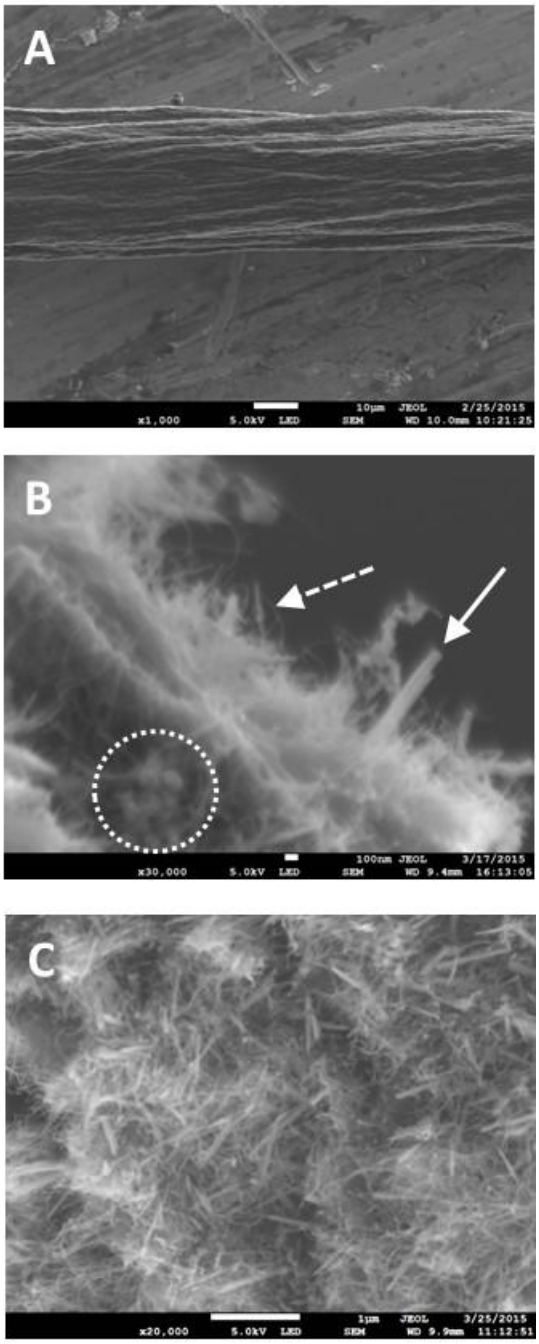
A
x1,000 5.0kV LED 10μm JEOL SEM WD 10.0mm 2/25/2015 10:21:25
B
x30,000 5.0kV LED 100nm JEOL SEM WD 9.4mm 3/17/2015 16:13:05
C
x20,000 5.0kV LED 1μm JEOL SEM WD 9.9mm 3/25/2015 11:12:51

**Figure 6**

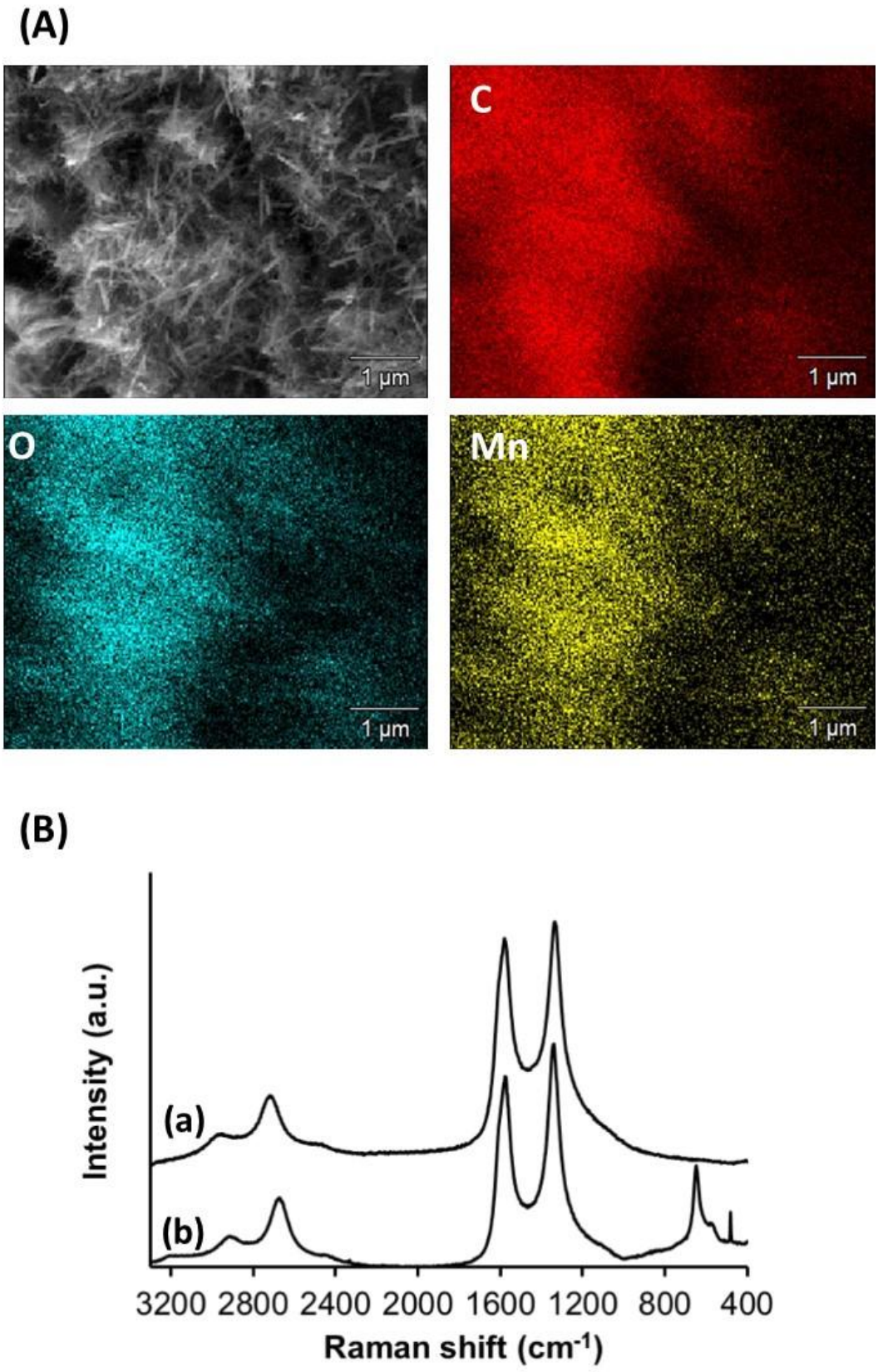
(A)
1 μm
C
1 μm
O
1 μm
Mn
1 μm
(B)
Intensity (a.u.)
(a)
(b)
3200 2800 2400 2000 1600 1200 800 400
Raman shift (cm-1)

**Figure 7**

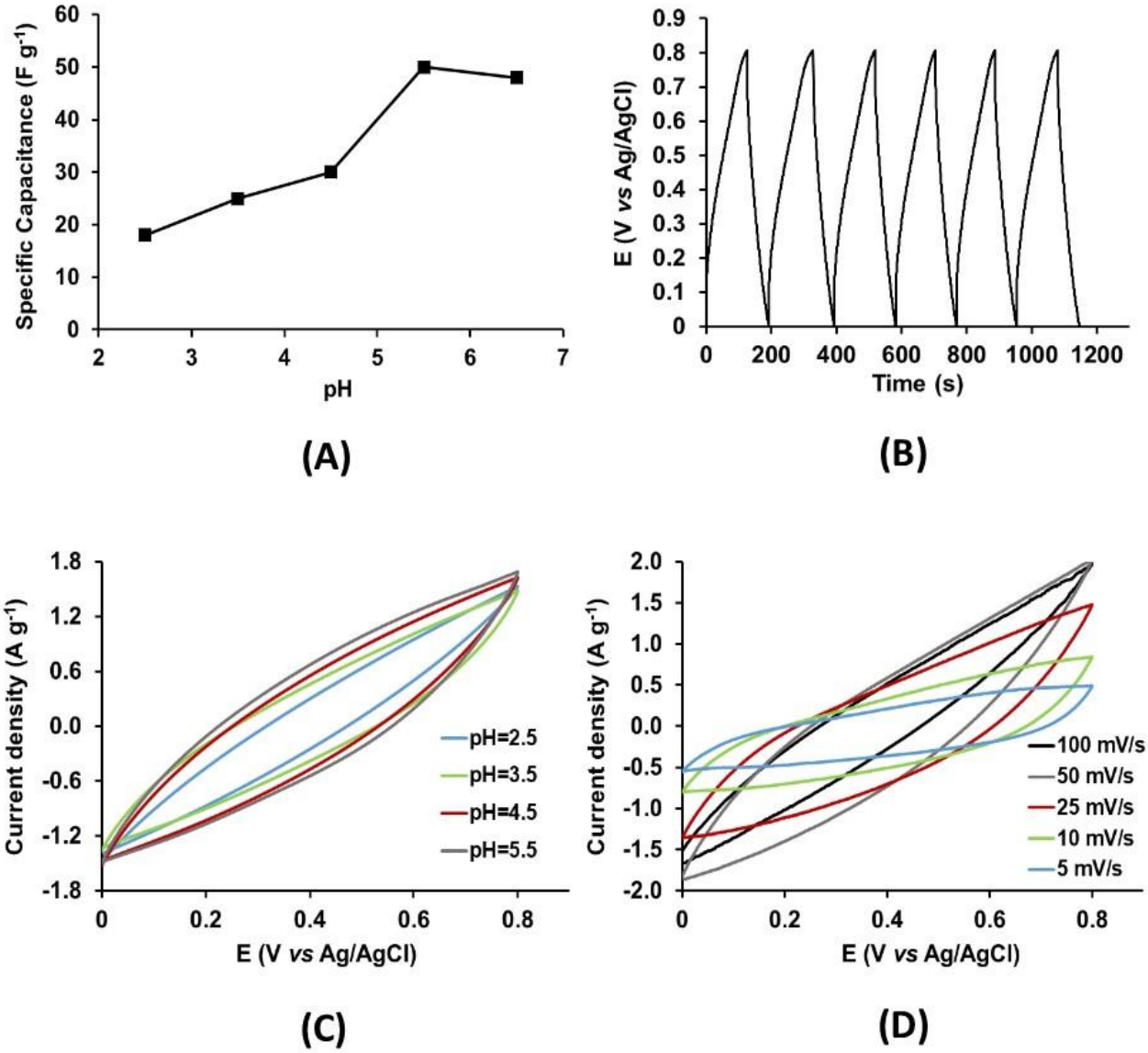
Specific Capacitance (F g-1)
pH
(A)
E (V vs Ag/AgCl)
Time (s)
(B)
Current density (A g-1)
E (V vs Ag/AgCl)
pH=2.5
pH=3.5
pH=4.5
pH=5.5
(C)
Current density (A g-1)
E (V vs Ag/AgCl)
100 mV/s
50 mV/s
25 mV/s
10 mV/s
5 mV/s
(D)

**Figure 8**

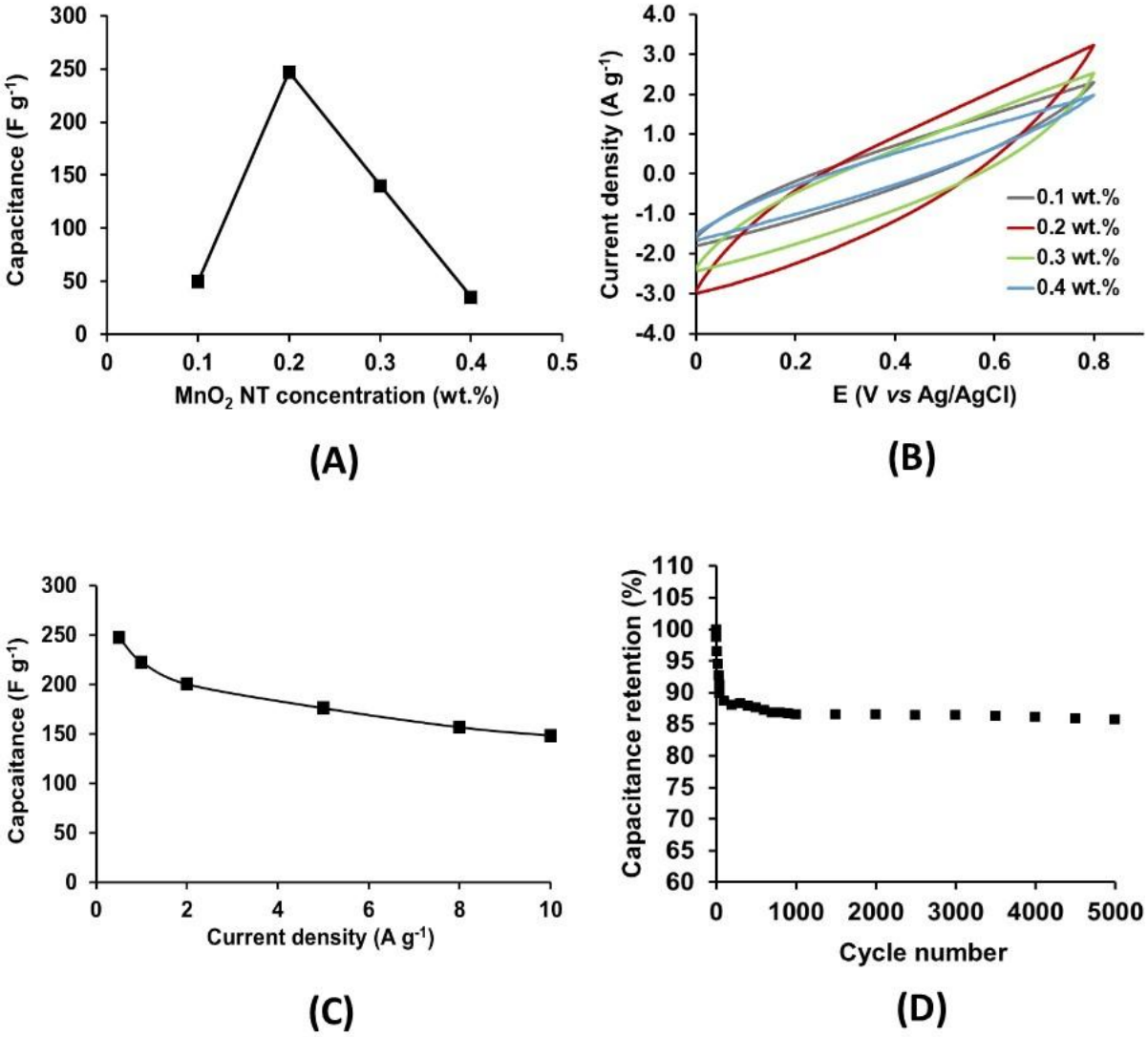
Capacitance (F g-1)
MnO2 NT concentration (wt.%)
(A)
Current density (A g-1)
E (V vs Ag/AgCl)
0.1 wt.%
0.2 wt.%
0.3 wt.%
0.4 wt.%
(B)
Capcaitance (F g-1)
Current density (A g-1)
(C)
Capacitance retention (%)
Cycle number
(D)

**Figure 9**